ACS OMEGA

http://pubs.acs.org/journal/acsodf

Article

Structural and Chemical Effects of the Surrounding Cations and Coexisting Compounds on $[M(\alpha\text{-}PW_{11}O_{39})_2]^{n-}$

Jun Iijima,* Haruo Naruke, and Ryuta X. Suzuki

Cite This: *ACS Omega* 2023, 8, 9673−9683

Read Online

ABSTRACT: The effects of countercations and coexisting compounds on the molecular structure of the $[M(\alpha\text{-}PW_{11}O_{39})_2]^{n-}$ polyanion were analyzed in terms of the repulsion and twisting of two $[\alpha\text{-}PW_{11}O_{39}]^{7-}$ units. More specifically, it was found that two $[\alpha\text{-}PW_{11}O_{39}]^{7-}$ ions approached one another upon reducing the ionic radius of M in $[M(\alpha\text{-}PW_{11}O_{39})_2]^{n-}$. The interactive twisting of the $[\alpha\text{-}PW_{11}O_{39}]^{7-}$ units prevented mutual repulsion of the units containing terminal O atoms, and the tendency for approach and twisting of the $[\alpha\text{-}PW_{11}O_{39}]^{7-}$ units varied as a function of the type of countercation and the presence of coexisting compounds. Overall, this study demonstrated that some interactions between the counteraction and coexisting compounds with $[M(\alpha\text{-}PW_{11}O_{39})_2]^{n-}$ determined the molecular conformation and the isolated form of the polyanion.

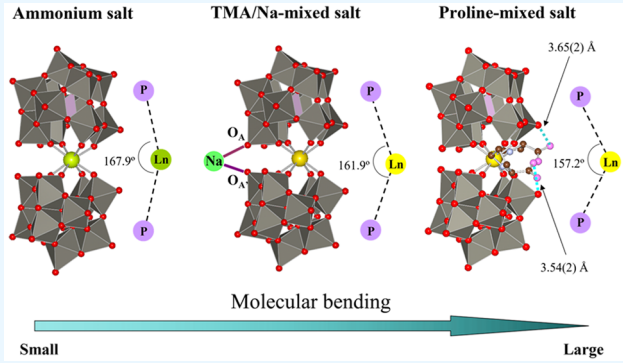

INTRODUCTION

Variation in the lanthanide linker ion (Ln) and the lacunary polyoxometalate (POM) building blocks has been demonstrated to produce numerous types of polyoxometallolanthanoates (Ln-POMs).[1−6] In addition to these compositional units, the synthetic conditions (e.g., stoichiometry, cationic species, reaction pH, and reaction temperature) also play strongly essential roles in the synthesis of Ln-POMs.[7] Since the discovery of sandwich-type Ln-POMs containing $Ln^{3+/4+}$ coordinated by two monolacunary Keggin $[XM_{11}O_{39}]^{n-}$, Wells−Dawson $[X_2M_{17}O_{61}]^{n-}$, or Lindqvist $[X_5O_{18}]^{n-}$ units by Peacock and Weakley in 1971,[5] intensive studies have been conducted on the structural chemistry and physicochemical properties of Ln-POMs.[8−18] In particular, in the cases of $[Ln(\alpha\text{-}PW_{11}O_{39})_2]^{11-}$ and $[Ln(\alpha_2\text{-}P_2W_{17}O_{61})_2]^{17-}$, which contain tetradentate monolacunary Keggin $[\alpha\text{-}PW_{11}O_{39}]^{7-}$ and Wells−Dawson $[\alpha_2\text{-}P_2W_{17}O_{61}]^{10-}$ units, respectively, the coordination mode of the central Ln^{3+} was studied by Fedotov and Francesconi using ^{31}P and ^{183}W NMR spectroscopy along with single crystal X-ray diffraction.[16,18] Their studies predicted that the $[Ln(\alpha\text{-}PW_{11}O_{39})_2]^{11-}$ and $[Ln(\alpha_2\text{-}P_2W_{17}O_{61})_2]^{17-}$ polyanions containing the Ln species in a cubic coordination environment exist only in solution, while those containing square-antiprismatic (SA) coordination environments are produced in the solid state. For the $[Ln(\alpha\text{-}PW_{11}O_{39})_2]^{11-}$ and $[Ln(\alpha_2\text{-}P_2W_{17}O_{61})_2]^{17-}$ polyanions, it can be easily imagined that their mirror planes halve the $[\alpha\text{-}PW_{11}O_{39}]^{7-}$ or $[\alpha_2\text{-}P_2W_{17}O_{61}]^{10-}$ units, respectively, and that the dihedral angle between the two mirror planes defines the molecular conformation and directs the coordination geometry of the central Ln ion. Indeed, ^{183}W NMR studies of $[Ln(\alpha\text{-}PW_{11}O_{39})_2]^{11-}$ in an aqueous solution suggested that the dihedral angle (φ) is dependent on the Ln species, wherein $\varphi = 0$ or 180° for Ln = La−Eu, and $0° < \varphi < 180°$ for Ln = Gd−Lu, thereby corresponding to cubic and SA coordination environments for Ln, respectively.[18] Since their experimental assumptions were consistent with theoretical discussions of the molecular structures of the $[Ln(\alpha\text{-}PW_{11}O_{39})_2]^{11-}$ and $[Ln(\alpha_2\text{-}P_2W_{17}O_{61})_2]^{17-}$ polyanions, it was considered that the molecular conformation of the Ln-POMs could be mainly explained based on the ionic radius of the Ln species (*i.e.*, Ln^{3+}). However, it is well-known that structural changes in the Ln-POMs are largely induced by countercations or coexisting compounds. To date, the effects of the cationic environment and the coexisting compounds on the molecular conformation of Ln-POMs have not been addressed in detail. However, we do note that our group previously demonstrated that both the cationic environment around the polyanion and the ionic size of the Ln^{3+} species of the polyanion play important roles in determining the conformation of $[Ln(\alpha\text{-}PW_{11}O_{39})_2]^{11-}$ and the coordination mode of Ln^{3+}.[19] For example, it was reported that the isotropic cationic environment caused by the

Received: February 3, 2023
Accepted: February 21, 2023
Published: March 3, 2023

Table 1. Crystallographic Data and Refinement Results of TN-Pr(III), TN-Eu(III), TN-Y(III), TN-Er(III), and aa-Ce(IV)-b

	TN-Pr(III)[c]	TN-Eu(III)[d]	TN-Er(III)[e]	TN-Y(III)[f]	aa-Ce(IV)-b[g]
empirical formula	$C_{24}H_{115}N_6O_{99.5}Na_5P_2W_{22}Pr$	$C_{24}H_{110}N_6O_{97}Na_5P_2W_{22}Eu$	$C_{24}H_{110}N_6O_{97}Na_5P_2W_{22}Er$	$C_{24}H_{117}N_6O_{100.5}Na_5P_2W_{22}Y$	$C_9H_{125}N_9O_{86}P_2W_{22}Ce$
formula wt	6441.61	6392.67	6422.97	6407.64	5927.39
crystal system	monoclinic	monoclinic	monoclinic	monoclinic	orthorhombic
space group	$P2/n$	$P2/n$	$P2/n$	$P2/n$	$P2_12_12_1$
a (Å)	13.2007(2)	13.0825(2)	13.3015(3)	13.2437(5)	12.2355(3)
b (Å)	12.6355(2)	12.6168(2)	12.6718(3)	12.6727(6)	22.2079(6)
c (Å)	35.4266(6)	35.2365(6)	34.9283(8)	35.0232(1)	34.6188(10)
β (deg)	98.1765(7)	97.799(7)	98.1051(8)	97.7508(1)	
V (A^3)	5848.96(2)	5762.3(2)	5828.5(2)	5824.4(4)	9406.8(4)
Z	2	2	2	2	4
θ range (deg)	3.1−27.5	3.4−68.2	3.0−27.7	3.0−27.5	3.0−27.5
limiting index reflections	$-17 \le h \le 17$	$-15 \le h \le 14$	$-17 \le h \le 17$	$-17 \le h \le 16$	$-15 \le h \le 14$
	$-16 \le k \le 15$	$-15 \le k \le 15$	$-14 \le k \le 16$	$-16 \le k \le 16$	$-28 \le k \le 28$
	$-45 \le l \le 45$	$-42 \le l \le 42$	$-45 \le l \le 45$	$-45 \le l \le 45$	$-44 \le l \le 44$
crystal size (mm^3)	0.28 × 0.28 × 0.13	0.40 × 0.20 × 0.08	0.38 × 0.24 × 0.20	0.25 × 0.19 × 0.08	0.61 × 0.21 × 0.12
D_c (g cm^{-3})	3.658	3.684	3.660	3.654	4.224
$F(000)$	5290.00	5336.00	5330.00	5282.00	10084.00
μ (mm^{-1})	22.1042	44.5190	22.4877	22.2841	27.4242
total data collected	89135	79920	79879	87046	151416
unique data	13371	10537	12667	13330	21522
R_{int}	0.1292	0.0705	0.0984	0.1120	0.1861
goodness of fit (GOF)	1.133	1.264	1.115	1.092	1.045
R1 ($I > 2\sigma(I)$)[a]	0.0600	0.0541	0.0599	0.0657	0.0569
wR2[b]	0.1488	0.1278	0.1386	0.1468	0.1379
Flack param					0.007(11)

[a]$R1 = (\sum|F_o| - F_c|)/(\sum|F_c|)$. [b]$wR2 = \sum[w(F_o^2 - F_c^2)^2]/\sum[w(F_o^2)^2]^{1/2}$. [c]$w$ (for **TN-Pr(III)**) $= 1/[\sigma^2(F_o^2) + (0.0001P)^2 + 222.4532P]$, where $P = (\mathrm{Max}(F_o^2,0) + 2F_c^2)/3$. [d]$w$ (for **TN-Eu(III)**) $= 1/[\sigma^2(F_o^2) + (0.0001P)^2 + 305.9653P]$, where $P = (\mathrm{Max}(F_o^2,0) + 2F_c^2)/3$. [e]$w$ (for **TN-Er(III)**) $= 1/[\sigma^2(F_o^2) + (0.0001P)^2 + 238.9383P]$, where $P = (\mathrm{Max}(F_o^2,0) + 2F_c^2)/3$. [f]$w$ (for **TN-Y(III)**) $= 1/[\sigma^2(F_o^2) + (0.0235P)^2 + 299.0283P]$, where $P = (\mathrm{Max}(F_o^2,0) + 2F_c^2)/3$. [g]$w$ (for **aa-Ce(IV)-b**) $= 1/[\sigma^2(F_o^2) + (0.0628P)^2 + 24.18103P]$, where $P = (\mathrm{Max}(F_o^2,0) + 2F_c^2)/3$.

tetramethylammonium cation (TMA) led to the first examples of $[Ln(\alpha\text{-}PW_{11}O_{39})_2]^{11-}$ (Ln = La, Ce) species exhibiting a cubic coordination center for LnO_8.[19] Thus, to achieve a targeted molecular design, it is necessary to investigate the relationship between the interactions of the surrounding cations and the coexisting compounds with Ln-POMs and their molecular conformations. In this study, we precisely analyze the molecular structures of the previously reported $[Ln(\alpha\text{-}PW_{11}O_{39})_2]^{11-}$ polyanion and examine the effects of the molecular environment (*i.e.*, cationic species and coexisting compounds) on the structure of the polyanion. It is expected that the obtained results will contribute to the molecular and functional design of Ln-POMs for use in future practical applications.

■ EXPERIMENTAL SECTION

Materials and Characterization. All chemicals were obtained commercially and were used without further purification. $Na_9[A\text{-}\alpha\text{-}PW_9O_{34}]\cdot 6H_2O$ was prepared according to a previously reported method and was identified by infrared (IR) spectroscopy according to the KBr disk method (Jasco FT/IR-410 spectrometer).[20] Elemental analyses (C, H, and N) were performed on Yanaco CHN Corder MT-5 and Vario EL III elemental analyzers. The contents of Ln (*i.e.*, Pr, Eu, Er, Y, and Ce), P, W, and Na were determined by inductively coupled plasma atomic emission spectroscopy (ICP-AES) on an ICPS-8100 spectrometer (Shimadzu) and a Spectro ICP Ciros CCD spectrometer. Thermogravimetric and differential thermal analyses (TG-DTA) were conducted using an ULVAC MTS9000 + TGD9600 system.

Syntheses. *$[Me_4N]_6Na_5[Pr(\alpha\text{-}PW_{11}O_{39})_2]\cdot 21.5H_2O$ (**TN-Pr-(III)**).* L-Proline (Pro; 0.173 g, 1.50 mmol) and $PrCl_3\cdot 7H_2O$ (0.187 g, 0.500 mmol) dissolved in H_2O (3 mL) were added to an aqueous solution of Me_4NCl (0.281 g, 2.50 mmol, 15 mL total volume). After heating at 60 °C for 30 min with stirring, the pH of the solution was adjusted to 1.5 using a 1 M aqueous HCl solution. Subsequently, an aqueous solution of $Na_9[A\text{-}\alpha\text{-}PW_9O_{34}]\cdot 6H_2O$ (2.43 g, 1.00 mmol, 20 mL) was added dropwise to the heated solution. After boiling for 1 h with stirring, the resulting solution was cooled to 25 °C and the residual powder was filtered off. The filtrate was then allowed to stand at room temperature for several days to yield light-green block crystals (0.771 g, 30.6% yield based on W). Found: C, 4.43; H, 1.37; N, 1.33; Na, 1.90; P, 0.95; W, 64.3; Pr, 1.97; H_2O, 6.05 wt %. Calcd for $C_{24}H_{115}N_6Na_5O_{99.5}P_2PrW_{22}$: C, 4.47; H, 1.80; N, 1.30; Na, 1.78; P, 0.96; W, 62.8; Pr, 2.19; H_2O, 6.01 wt %. IR (KBr disk) cm^{-1}: 1485s, 1094s, 1045s, 950vs, 891m, 836m, 779s, 741w, 614w, 517w.

*$[Me_4N]_6Na_5[Eu(\alpha\text{-}PW_{11}O_{39})_2]\cdot 19H_2O$ (**TN-Eu(III)**).* The procedure described for the preparation of **TN-Pr(III)** was also applied to the preparation of **TN-Eu(III)** using $EuCl_3\cdot 6H_2O$ (0.184 g, 0.500 mmol) instead of $PrCl_3\cdot 7H_2O$ to obtain colorless block crystals (1.21 g, 48.3% yield based on W). Found: C, 4.39; H, l.29; N, 1.25; Na, 1.99; P, 0.86; W, 65.4; Eu, 2.16; H_2O, 5.39 wt %. Calcd for $C_{24}H_{110}N_6Na_5O_{97}P_2EuW_{22}$: C, 4.50; H, 1.73; N, 1.31; Na, 1.79; P, 0.97; W, 63.1; Eu, 2.37; H_2O, 5. 34 wt %. IR (KBr

https://doi.org/10.1021/acsomega.3c00711
ACS Omega 2023, 8, 9673−9683

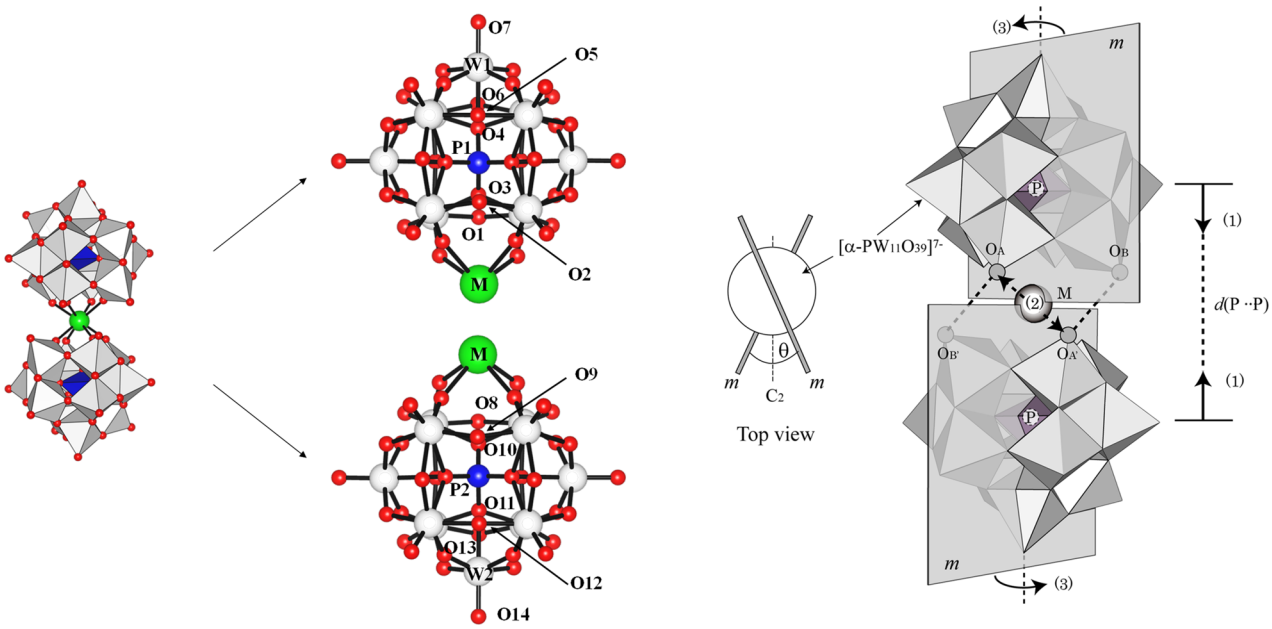

Figure 1. Combined polyhedral and ball-and-stick representation of $[M(\alpha\text{-}PW_{11}O_{39})_2]^{n-}$ viewed along the C_2 axis (left). Color scheme: WO_6, white octahedra; PO_4, blue tetrahedra; O atoms, red spheres; M atoms, green spheres. Labeling of the atoms defining the mirror planes of the monolacunary Keggin $[\alpha\text{-}PW_{11}O_{39}]^{7-}$ unit (middle). Schematic drawing (right) of $[M(\alpha\text{-}PW_{11}O_{39})_2]^{n-}$ viewed along the C_2 axis, exhibiting the relationship between the ionic radius of M (R_M) and twist angle (ϕ): (1) the decrease in P···P distance (d(P···P)) with decreasing R_M; (2) the decreased in O_A···$O_{A'}$ distance (d(P···P)) with decreasing (d(P···P)); (3) the mirror planes (m) in the $[\alpha\text{-}PW_{11}O_{39}]^{7-}$ unit rotating in the ϕ-decreasing direction to diminish the O_A···$O_{A'}$ repulsion.

disk) cm^{-1}: 1485s, 1099s, 1047s, 951vs, 889m, 839m, 781s, 745w, 595w, 518w.

*$[Me_4N]_6Na_5[Er(\alpha\text{-}PW_{11}O_{39})_2]\cdot 19H_2O$ (**TN-Er(III)**).* The procedure described for the preparation of **TN-Pr(III)** was also applied to the preparation of **TN-Er(III)** using $ErCl_3\cdot 6H_2O$ (0.191 g, 0.500 mmol) instead of $PrCl_3\cdot 7H_2O$ to obtain light-pink block crystals (0.753 g, 30.0% yield based on W). Found: C, 4.30; H, 1.31; N, 1.29; Na, 1.93; P, 0.83; W, 63.2; Er, 2.59; H_2O, 5.27 wt %. Calcd for $C_{24}H_{110}N_6Na_5O_{97}P_2ErW_{22}$: C, 4.49; H, 1.73; N, 1.31; Na, 1.79; P, 0.96; W, 63.0; Er, 2.60; H_2O, 5.33 wt %. IR (KBr disk) cm^{-1}: 1485s, 1106s, 1047m, 952vs, 891m, 842m, 782s, 754w, 610w, 517w.

*$[Me_4N]_6Na_5[Y(\alpha\text{-}PW_{11}O_{39})_2]\cdot 22.5H_2O$ (**TN-Y(III)**).* The procedure described for the preparation of **TN-Pr(III)** was also applied to the preparation of **TN-Y(III)** using $YCl_3\cdot 6H_2O$ (0.152 g, 0.500 mmol) instead of $PrCl_3\cdot 7H_2O$ to obtain white block crystals (0.892 g, 35.6% yield based on W). Found: C, 4.38; H, 1.30; N, 1.34; Na, 1.82; P, 0.98; W, 63.3; Y, 1.37; H_2O, 6.17 wt %. Calcd for $C_{24}H_{117}N_6Na_5O_{100.5}P_2YW_{22}$: C, 4.50; H, 1.84; N, 1.31; Na, 1.79; P, 0.97; W, 63.1; Y, 1.39; H_2O, 6.33 wt %. IR (KBr disk) cm^{-1}: 1484s, 1449w, 1414w, 1367w, 1329w, 1284w, 1228w, 1105s, 1048s, 952vs, 892m, 843w, 827w, 780m, 738w, 596w, 518m.

*$[MeNH_3]_9H[Ce(\alpha\text{-}PW_{11}O_{39})_2]\cdot 8H_2O$ (**aa-Ce(IV)-b**).* $(NH_4)_4Ce(SO_4)_4\cdot 4H_2O$ (0.671 g, 1.00 mmol) was dissolved in H_2O (20 mL), and the pH of the solution was adjusted to 1.5 using a 1 M aqueous solution of HCl. Subsequently a solution of $Na_9[A\text{-}\alpha\text{-}PW_9O_{34}]\cdot 6H_2O$ (2.57 g, 1.00 mmol) in H_2O (10 mL) was added, and the resulting solution was boiled for 1 h with stirring. After this time, the mixture was cooled to 25 °C and the residual powder was filtered. $MeNH_3\cdot HCl$ (0.810 g, 12.0 mmol) dissolved in H_2O (5 mL) was then added to the filtrate, and the solution was heated at 60 °C for 30 min with stirring. After cooling to room temperature, the residual powder was removed by filtration, and the filtrate was allowed to stand for several months to yield yellow needle-like crystals (0.971 g, 39.6% yield based on W). Found: C, 2.30; H, 1.44; N, 2.30; P, 1.28; W, 83.9; Ce, 2.95; H_2O, 5.27 wt %. Calcd for $C_9H_{71}N_9O_{86}P_2CeW_{22}$: C, 2.62; H, 1.21; N, 2.13; P, 1.04; W, 84.8; Ce, 2.97; H_2O, 5.31 wt %. IR (KBr disk) cm^{-1}: 1496w, 1460w, 1424w, 126lw, 1102m, 1052m, 957vs, 883m, 807s, 737s, 505w.

Single-Crystal X-ray Crystallography. Single-crystal X-ray diffraction analysis was carried out for all compounds using a Rigaku RAXIS-RAPID imaging plate diffractometer with graphite-monochromatized Mo Kα radiation (λ = 0.7107 Å) at 183−213 K. A numerical absorption correction was then performed for all compoundsusing SHAPE[21] and NUMABS.[22] The structures were solved by direct methods with SHELXS-2013/1[23] and refined using the full-matrix least-squares program SHELXL-2014/6[24] on F^2 with the CrystalStructure 4.3.2 crystallographic software package.[25] The Ln (Pr, Eu, Er, Y, and Ce), W, P, and Na elements were refined anisotropically, while C, N, and O were refined isotropically. The H atoms were not included in the refinements.[26] The absolute structure of **aa-Ce(IV)-b** was determined using Flack parameter refinement.[27] The squeeze program was performed on **TN-Eu(III)**, **-Er(III)**, and **-Y(III)**.[28] Further details regarding the crystal structures can be obtained from the Cambridge Crystallographic Data Center (CCDC) under depository numbers CCDC-812378 (**TN-Pr(III)**), CCDC-1945568 (**TN-Eu(III)**), CCDC-812380 (**TN-Er(III)**), CCDC-1936822 (**TN-Y(III)**), and CCDC-2008002 (**aa-Ce-(IV)-b**). The crystallographic data and results of the structural refinements are summarized in Table 1.

Classification and Definition of the Structural Parameters of $[M(\alpha\text{-}PW_{11}O_{39})_2]^{n-}$. For the purpose of this study, we evaluated 30 $[M(\alpha\text{-}PW_{11}O_{39})_2]^{n-}$ polyanions with

https://doi.org/10.1021/acsomega.3c00711
ACS Omega 2023, 8, 9673−9683

Table 2. Comparison of the Structural Parameters for the Pure Alkylammonium Salt Family, TMA^+/Na^+-Mixed Salt Family, and Na^+/K^+-Mixed Salt Family

M in $[M(\alpha\text{-}PW_{11}O_{39})_2]^{n-}$	abbreviation	cation	R_M (Å)[a]	d(P···P) (Å)[b]	$d(O_A\cdots O_{A'})$ (Å)[c]	$d(O_A\cdots O_{B'})$ (Å)[c]	$d(O_A\cdots O_B)$ (Å)[c]	ϕ (deg)[d]
			Pure Alkylammonium Salt					
Ce(III)	**aa-Ce(III)**	$[Me_2NH_2]^+$	1.143	9.067	3.286	4.501(9)	4.561(8)	42.9
Ce(IV)	**aa-Ce(IV)-a**	$[Me_2NH_2]^+$	0.97	8.743	2.923	3.747(7)	3.723(4)	40.2
Ce(IV)	**aa-Ce(IV)-b**	$[MeNH_3]^+$, H^+	0.97	8.747	2.940	3.770(0)	3.730(0)	41.0
Hf(IV)	**aa-Hf(IV)**	$[Me_2NH_2]^+$	0.83	8.511	2.772	3.200(2)	3.200(2)	37.5
Zr(IV)	**aa-Zr(IV)-L**	$[Me_2NH_2]^+$	0.84	8.550	2.855	3.315(9)	3.302(7)	37.8
Zr(IV)	**aa-Zr(IV)-R**	$[Me_2NH_2]^+$	0.84	8.558	2.862	3.284(6)	2.394(4)	38.1
Hf(IV)	**aa-Hf(IV)-1**	$[Et_2NH_2]^+$	0.83	8.514	2.931	3.137(9)	3.127(6)	35.9
Hf(IV)	**aa-Hf(IV)-2**	$[Et_2NH_2]^+$	0.83	8.595	2.909	3.423(3)	3.304(8)	38.2
Zr(IV)	**aa-Zr(IV)-1**	$[Et_2NH_2]^+$	0.84	8.558	2.935	3.253(0)	3.047(8)	35.9
Zr(IV)	**aa-Zr(IV)-2**	$[Et_2NH_2]^+$	0.84	8.612	2.914	3.268(4)	3.429(0)	37.9
			TMA^+/Na^+-Mixed Salts					
Pr(III)	**TN-Pr(III)-p**	Na^+, $[Me_4N]^+$, H^+	1.126	8.939	3.408	3.508(7)	3.508(7)	33.4
Pr(III)	**TN-Pr(III)**	Na^+, $[Me_4N]^+$	1.126	8.986	3.374	3.609(8)	3.609(8)	33.5
Eu(III)	**TN-Eu(III)**	Na^+, $[Me_4N]^+$	1.066	8.894	3.305	3.517(5)	3.517(5)	33.8
Y(III)	**TN-Y(III)**	Na^+, $[Me_4N]^+$	1.019	8.850	3.211	3.438(9)	3.438(9)	33.3
Er(III)	**TN-Er(III)**	Na^+, $[Me_4N]^+$	1.004	8.831	3.270	3.406(5)	3.406(5)	33.4
Ce(IV)	**TN-Ce(IV)**	Na^+, $[Me_4N]^+$, NH_4^+	0.97	9.016	3.480	3.539(6)	3.539(6)	32.1
			Na^+/K^+-Mixed Salts Containing Pro					
La(III)	**NK-La(III)-L**	Na^+, K^+, H^+	1.160	8.936	3.063	3.543(2)	3.437(9)	36.0
Pr(III)	**NK-Pr(III)-L**	Na^+, K^+, H^+	1.126	8.862	2.986	3.440(2)	3.481(1)	34.9
Pr(III)	**NK-Pr(III)-D**	Na^+, K^+, H^+	1.126	8.851	3.017	3.398(1)	3.445(0)	34.5
Nd(III)	**NK-Nd(III)-L**	Na^+, K^+, H^+	1.109	8.827	3.021	3.405(2)	3.455(3)	34.8
Sm(III)	**NK-Sm(III)-L**	Na^+, K^+, H^+	1.079	8.798	2.974	3.374(4)	3.465(3)	35.0
Eu(III)	**NK-Eu(III)-L**	Na^+, K^+, H^+	1.066	8.791	2.983	3.353(9)	3.400(1)	35.1
Gd(III)	**NK-Gd(III)-L**	Na^+, K^+, H^+	1.053	8.780	2.955	3.392(0)	3.410(7)	36.0
Tb(III)	**NK-Tb(III)-L**	Na^+, K^+, H^+	1.040	8.797	2.961	3.349(6)	3.420(7)	35.2
Dy(III)	NK-Dy(III)-L	Na^+, K^+, H^+	1.027	8.770	2.871	3.368(6)	3.400(6)	35.0
Y(III)	**NK-Y(III)-L**	Na^+, K^+, H^+	1.019	8.731	2.897	3.346(5)	3.389(3)	35.2
Er(III)	**NK-Er(III)-L**	Na^+, K^+, H^+	1.004	8.731	2.939	3.338(6)	3.338(5)	35.5
Er(III)	**NK-Er(III)-D**	Na^+, K^+, H^+	1.004	8.724	2.876	3.366(3)	3.363(2)	34.7
Tm(III)	**NK-Tm(III)-L**	Na^+, K^+, H^+	0.994	8.711	2.877	3.314(3)	3.308(1)	34.7
Yb(III)	**NK-Yb(III)-L**	Na^+, K^+, H^+	0.985	8.735	2.919	3.330(2)	3.397(1)	34.9

[a] R_M: ionic radius of M from ref 36. [b] d(P···P): distance between P atoms belonging to two monolacunary Keggin units represented in Figure 1 (right). [c] $d(O_A\cdots_{A'})$, $d(O_A\cdots O_{B'})$, $d(O_{A'}\cdots O_B)$: distances between terminal O atoms represented in Figure 1 (right). [d] ϕ: twist angle between the two mirror planes of monolacunary Keggin units represented in Figure 1 (right).

different cationic species and coexisting compounds. To discuss the structural and chemical effects of these species on the $[M(\alpha\text{-}PW_{11}O_{39})_2]^{n-}$ polyanion crystals, the 30 compounds were classified into three families: namely, pure alkylammonium salts (**aa-M(III/IV)-a/b/1/2/R/L**), TMA^+/Na^+-mixed salts (**TN-M(III/IV)**), and $Na^+/K^+/H^+$-mixed salts (**NK-M(III)-L/D**). It should be noted that the **aa-M(III/IV)-a/b/1/2/R/L** family includes ten compounds, such as the monomethylammonium salt of $[Ce^{IV}(\alpha\text{-}PW_{11}O_{39})_2]^{10-}$, dimethylammonium salts of $[M(\alpha\text{-}PW_{11}O_{39})_2]^{n-}$ (M = Ce^{III}, Ce^{IV}, Hf^{IV}, and Zr^{IV}),[29−31] and diethylammonium salts of $[M(\alpha\text{-}PW_{11}O_{39})_2]^{n-}$ (M = Hf^{IV} and Zr^{IV}).[32] In addition, the **TN-M(III/IV)** family consists of six compounds, including TMA^+/Na^+-mixed salts of $[M(\alpha\text{-}PW_{11}O_{39})_2]^{n-}$ (M = Pr^{III}, Eu^{III}, Y^{III}, and Er^{III}) and $TMA^+/Na^+/NH_4^+$-mixed salts of $[Ce^{IV}(\alpha\text{-}PW_{11}O_{39})_2]^{10-}$.[33] Furthermore, the **NK-M(III)-L/D** family contains 14 compounds, such as the Pro-containing $Na^+/K^+/H^+$-mixed salts of $[M(\alpha\text{-}PW_{11}O_{39})_2]^{n-}$ (M= La^{III}, Pr^{III}, Nd^{III}, Sm^{III}, Eu^{III}, Gd^{III}, Tb^{III}, Dy^{III}, Y^{III}, Er^{III}, Tm^{III}, and Yb^{III}).[34,35]

Five structural parameters were introduced for $[M(\alpha\text{-}PW_{11}O_{39})_2]^{n-}$: namely, R_M, d(P···P), d(O···O), φ, and ϕ (see Figure 1 (right)). More specifically, R_M is the ionic radius of M with a coordination number of 8 in $[M(\alpha\text{-}PW_{11}O_{39})_2]^{n-}$,[36] and d(P···P) is defined as the distance between two P atoms in $[M(\alpha\text{-}PW_{11}O_{39})_2]^{n-}$; this parameter describes the degree of separation between the two $[\alpha\text{-}PW_{11}O_{39}]^{7-}$ units. In addition, d(O···O) is defined by the three O···O distances (*i.e.*, $O_A\cdots O_{A'}$, $O_A\cdots O_{B'}$, and $O_{A'}\cdots O_B$) between the two terminal O atoms in two $[\alpha\text{-}PW_{11}O_{39}]^{7-}$ units of $[M(\alpha\text{-}PW_{11}O_{39})_2]^{n-}$; this is an important parameter for understanding the degree of steric repulsion between the two $[\alpha\text{-}PW_{11}O_{39}]^{7-}$ units. Furthermore, ϕ is the twist angle between the two $[\alpha\text{-}PW_{11}O_{39}]^{7-}$ units. The twist angle is defined as the dihedral angle between the two least-squares planes determined by the M atom, 1 of 11 W atoms, the P atom, and 7 bridging O atoms. These atoms are denoted as [M, W^1, P^1, O^{1-7}] and [M, W^2, P^2, O^{8-14}], respectively, as shown in Figure 1 (middle). This least-squares plane is the mirror plane, which halves the C_s-symmetric $[\alpha\text{-}PW_{11}O_{39}]^{7-}$ unit in $[M(\alpha\text{-}PW_{11}O_{39})_2]^{n-}$. This parameter allows us to understand both the approach of the two $[\alpha\text{-}PW_{11}O_{39}]^{7-}$ units and the repulsion attributed to O···O interactions. Moreover, φ is the ∠P−M−P bending angle and provides the degree of

https://doi.org/10.1021/acsomega.3c00711
ACS Omega 2023, 8, 9673−9683

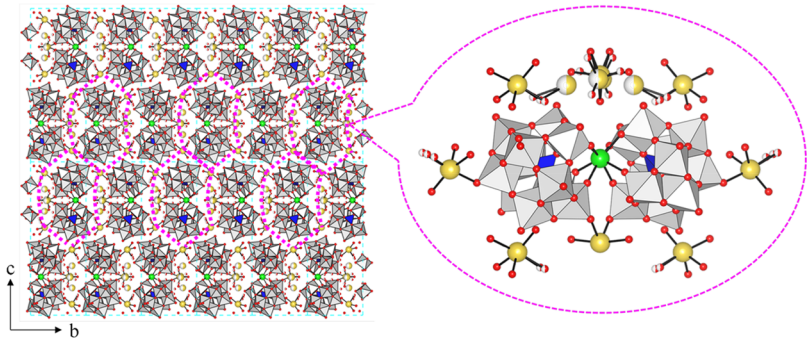

Figure 2. Crystal structure of **TN-Pr(III)** projected on the *bc* plane (left). Shown on the right is an enlarged picture of the crystal structure on the left circled by a pink dotted line. Two $[\alpha\text{-PW}_{11}\text{O}_{39}]^{7-}$ units in the polyanion in the pink dotted line are locked by a Na^+ cation.

bending of $[M(\alpha\text{-PW}_{11}\text{O}_{39})_2]^{n-}$. The various parameters for the 30 polyanions are summarized in Table 2.

■ RESULTS AND DISCUSSION

Crystal Structures of TN-Ln(III) (Ln = Pr, Eu, Er, or Y) and aa-Ce(IV)-b. The prepared **TN-Pr(III)**, **TN-Eu(III)**, **TN-Er(III)**, and **TN-Y(III)** are isomorphous species that crystallized in the monoclinic space group *P*2/*n*. These complexes are composed of six $[Me_4N]^+$ cations, five Na^+ cations, the $[M(\alpha\text{-PW}_{11}\text{O}_{39})_2]^{11-}$ anion (M = Pr, Eu, Er, or Y), and some crystallized water molecules. In contrast, **aa-Ce(IV)-b**, which was obtained from spontaneous resolution without the use of a chiral auxiliary such as $[Me_2NH_2]_{10}[Ce^{IV}(\alpha\text{-PW}_{11}\text{O}_{39})_2]\cdot 14H_2O$,[29] $[Me_2NH_2]_{10}[Hf^{IV}(\alpha\text{-PW}_{11}\text{O}_{39})_2]\cdot 8H_2O$,[30] or $[Me_2NH_2]_{10}[Zr^{IV}(\alpha\text{-PW}_{11}\text{O}_{39})_2]\cdot 10H_2O$,[31] crystallized in the orthorhombic space group $P2_12_12_1$. This complex is composed of nine $[MeNH_3]^+$ cations, one proton (H^+), the $[Ce(\alpha\text{-PW}_{11}\text{O}_{39})_2]^{10-}$ anion, and some crystallized water molecules. As shown in Figure 1 (left-hand panel), the polyanions are also composed of two monolacunary Keggin $[\alpha\text{-PW}_{11}\text{O}_{39}]^{7-}$ units sandwiching the M^{n+} ions in a SA coordination environment, resulting in molecular C_2 symmetry. The M−O bond lengths were determined to be in the range of 2.45(1)−2.48(1) Å for **TN-Pr(III)**, 2.39(1)−2.41(2) Å for **TN-Eu(III)**, 2.33(1)−2.37(1) Å for **TN-Er(III)**, 2.34(1)−2.38(1) Å for **TN-Y(III)**, and 2.31(2)−2.38(2) Å for **aa-Ce(IV)-b**. These values are comparable to those in $[Pr^{III}(W_5O_{18})_2]^{9-}$ (2.43(2)−2.54(2) Å, average 2.48 Å),[9] $[Eu^{III}(W_5O_{18})_2]^{9-}$ (2.40(3)−2.46(3) Å, average 2.43 Å),[10] $[Er^{III}(W_5O_{18})_2]^{9-}$ (2.34(1)−2.39(1) Å, average 2.37 Å),[11] $[(YOH_2)_3(CO_3)(A\text{-}\alpha\text{-PW}_9\text{O}_{34})_2]^{11-}$ (2.22(2)−2.46(1) Å, average 2.32 Å),[37] and $[Ce^{IV}(\alpha\text{-PW}_{11}\text{O}_{39})_2]^{10-}$ (2.30(2)−2.38(2) Å, average 2.38 Å).[8] The BVS values[38] calculated from the observed bond lengths were as follows: 3.0 for Pr, 5.0 for P, and 5.8−6.2 for W in **TN-Pr(III)**; 3.0 for Eu, 4.9 for P, and 5.8−6.0 for W in **TN-Eu(III)**; 3.0 for Er, 4.9 for P, and 5.8−6.1 for W in **TN-Er(III)**; 3.1 for Y, 5.0 for P, and 5.9−6.1 for W in **TN-Y(III)**; 3.8 for Ce, 5.0−5.1 for P, and 5.8−6.1 for W in **aa-Ce(IV)-b**. These values are consistent with the original valences of Pr^{3+}, Eu^{3+}, Er^{3+}, Y^{3+}, Ce^{4+}, P^{5+}, and W^{6+}.

Figure 2 (left panel) shows the crystal structure of **TN-Pr(III)** projected onto the *bc* plane, wherein it can be seen that the polyanions are surrounded by nondisordered and partially disordered Na^+ ions in a ring-shaped arrangement (pink dotted lines). Because of the presence of these Na^+ cations, the TMA^+ cations around the polyanion are positioned asymmetrically. Similar to the structure of $[Me_4N]_4Na_3H_4[Pr(\alpha\text{-PW}_{11}\text{O}_{39})_2]\cdot 12H_2O$ reported by Fan et al.,[39] one of the Na^+ cations (circled in blue) connects the two $[\alpha\text{-PW}_{11}\text{O}_{39}]^{7-}$ units of $[Pr(\alpha\text{-PW}_{11}\text{O}_{39})_2]^{11-}$ via O−Na−O bonding, thereby locking a twist of the $[\alpha\text{-PW}_{11}\text{O}_{39}]^{7-}$ units and extending the molecular length of the $[Pr(\alpha\text{-PW}_{11}\text{O}_{39})_2]^{11-}$ polyanion, as shown in Figure 2 (right panel). In addition, Figure 3 shows the crystal structure of **aa-Ce(III)-b** projected onto the *bc* plane. Similar to the structure of $[Me_2NH_2]_{10}[Ce^{IV}(\alpha\text{-PW}_{11}\text{O}_{39})_2]\cdot 14H_2O$,[29] the polyanion is surrounded by $[MeNH_3]^+$ cations and some crystallization water molecules, resulting in the generation of a three-dimensional (3D) network based on hydrogen-bonding interactions in the crystal structure.

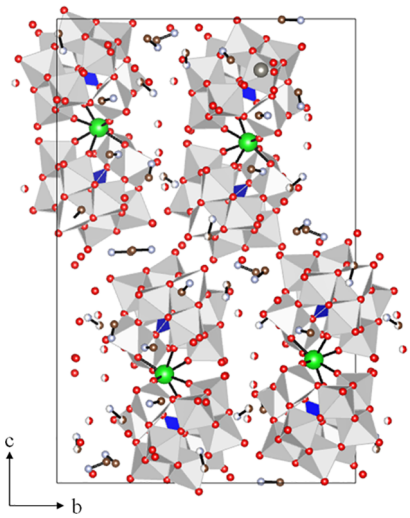

Figure 3. Crystal structure of **aa-Ce(IV)-b** projected on the *bc* plane. The crystallized $[MeNH_3]^+$ cations and some waters of crystallization form a 3D network space, spreading weak hydrogen-bonding interactions.

Structural Evaluation of the Pure Alkylammonium Salt Family. Figure 4 shows the relationship among the selected geometric parameters of the pure alkylammonium salt family, whose members include $[Me_2NH_2]_{11}[Ce^{III}(\alpha\text{-PW}_{11}\text{O}_{39})_2]\cdot 14H_2O$ (**aa-Ce(III)**),[29] $[Me_2NH_2]_{10}[Ce^{IV}(\alpha\text{-PW}_{11}\text{O}_{39})_2]\cdot 14H_2O$ (**aa-Ce(IV)-a**),[29] $[MeNH_3]_9H[Ce(\alpha\text{-PW}_{11}\text{O}_{39})_2]\cdot 8H_2O$ (**aa-Ce(IV)-b**), $[Me_2NH_2]_{10}[Hf^{IV}(\alpha\text{-PW}_{11}\text{O}_{39})_2]\cdot 8H_2O$ (**aa-Hf(IV)**),[30] $[Me_2NH_2]_{10}[Zr^{IV}(\alpha\text{-PW}_{11}\text{O}_{39})_2]\cdot 7H_2O$ (**aa-Zr(IV)-L** and **-R**),[31] $[Et_2NH_2]_{10}[Hf^{IV}(\alpha\text{-PW}_{11}\text{O}_{39})_2]\cdot 2H_2O$ (**aa-Hf(IV)-1** and **2**),[31] and $[Et_2NH_2]_{10}[Zr^{IV}(\alpha\text{-PW}_{11}\text{O}_{39})_2]\cdot 7H_2O$ (**aa-Zr(IV)-1** and **2**) (see also Table 2).[32] As shown in Figure 4a, *d*(P···P)

https://doi.org/10.1021/acsomega.3c00711
ACS Omega 2023, 8, 9673−9683

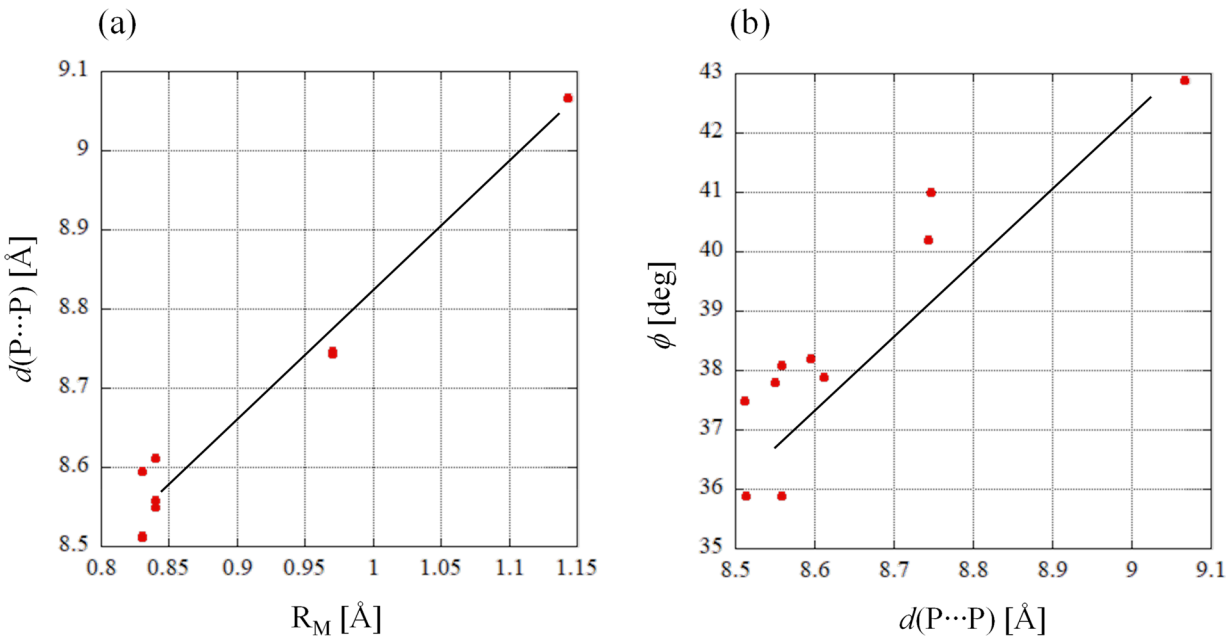

Figure 4. Plots of the (a) ionic radius of M (R_M) versus P···P distance (d(P···P)) and (b) d(P···P) versus the twist angle (ϕ) for the $[M(\alpha\text{-}PW_{11}O_{39})_2]^{n-}$ polyanion in the pure alkylammonium salt family given in Table 2. The solid line in each plot is drawn to guide the correlation.

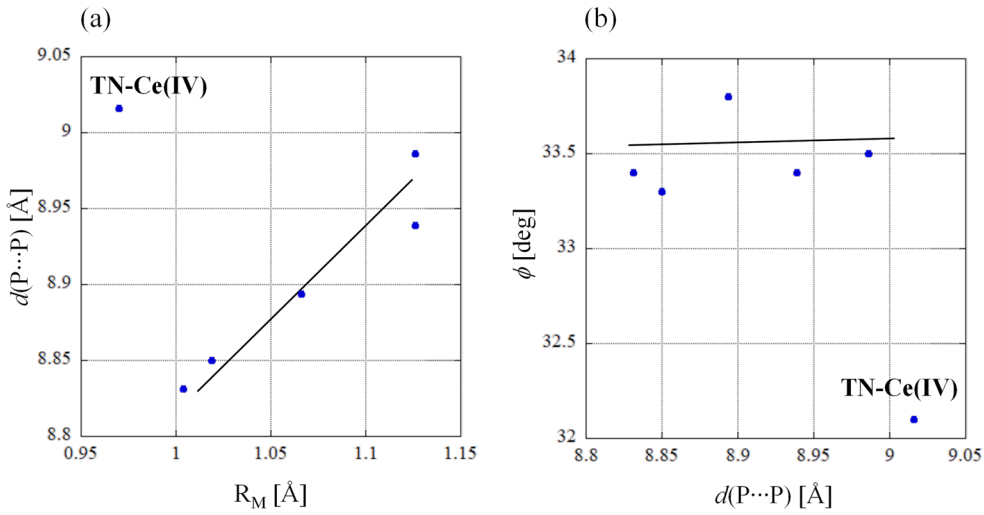

Figure 5. Plots of the (a) ionic radius of M (R_M) versus P···P distance (d(P···P)) and (b) d(P···P) versus twist angle (ϕ) for the $[M(\alpha\text{-}PW_{11}O_{39})_2]^{n-}$ polyanion in the TMA^+/Na^+-mixed salt family given in Table 2. The solid line in each plot is drawn to guide the correlation.

tends to increase with an increase in R_M owing to stretching of the M−O bonds. In addition, Figure 4b shows that φ decreases as the two $[\alpha\text{-}PW_{11}O_{39}]^{7-}$ units approach one another, and this behavior can be reasonably explained in terms of the repulsive interactions between the O atoms of the two $[\alpha\text{-}PW_{11}O_{39}]^{7-}$ units. Furthermore, Figure 1 (right panel) shows a schematic representation of the $[M(\alpha\text{-}PW_{11}O_{39})_2]^{n-}$ polyanion, in which the three short O···O contacts are denoted as $O_A\cdots O_{A'}$, $O_A\cdots O_{B'}$, and $O_{A'}\cdots O_B$. Table 2 gives their $d(O_A\cdots O_{A'})$, $d(O_A\cdots O_{B'})$, and $d(O_{A'}\cdots O_B)$ distances, of which $d(O_A\cdots O_{A'})$ is the shortest and decreases with a decreasing value of d(P···P). For the $[Hf^{IV}(\alpha\text{-}PW_{11}O_{39})_2]^{10-}$ polyanions in **aa-Hf(IV)-1** and **-2**, the $d(O_A\cdots O_{A'})$ values are particularly short (2.77−2.93 Å) and correspond to approximately double the ionic radius of O^{2-} (i.e., 1.35 × 2 = 2.70 Å),[36] thereby suggesting a remarkable repulsion acting between the O_A and $O_{A'}$ atoms. Figure 1 (right panel) also shows how the approach of the $[\alpha\text{-}PW_{11}O_{39}]^{7-}$ units lowers ϕ through $O_A\cdots O_{A'}$ repulsion, *i.e.*, a decrease in R_M results in a mutual approach of the $[\alpha\text{-}PW_{11}O_{39}]^{7-}$ units (Figure 4a) and a remarkable repulsion between the O_A and $O_{A'}$ atoms. This steric repulsion was reduced by a decrease in ϕ (Figure 4b). Due to the fact that the $[M(\alpha\text{-}PW_{11}O_{39})_2]^{n-}$ polyanions in pure alkylammonium salts are weakly hydrogen-bonded by alkylammonium cations and water molecules, it is therefore suggested that their conformations are influenced to a lesser extent by the surroundings of the polyanion and are mainly controlled by intramolecular repulsion.

Structural Evaluation of the TMA^+/Na^+-Mixed Salt Family. Figure 5 shows the relationship among the structural parameters of the TMA^+/Na^+-mixed salt family, namely $[Me_4N]_4Na_3H_4[Pr(a\text{-}PW_{11}O_{39})_2]\cdot 12H_2O$ (**TN-Pr(III)-p**),[39] $[Me_4N]_6Na_5[Pr(\alpha\text{-}PW_{11}O_{39})_2]\cdot 21.5H_2O$ (**TN-Pr(III)**), $[Me_4N]_6Na_5[Eu(\alpha\text{-}PW_{11}O_{39})_2]\cdot 19H_2O$ (**TN-Eu(III)**),

https://doi.org/10.1021/acsomega.3c00711
ACS Omega 2023, 8, 9673−9683

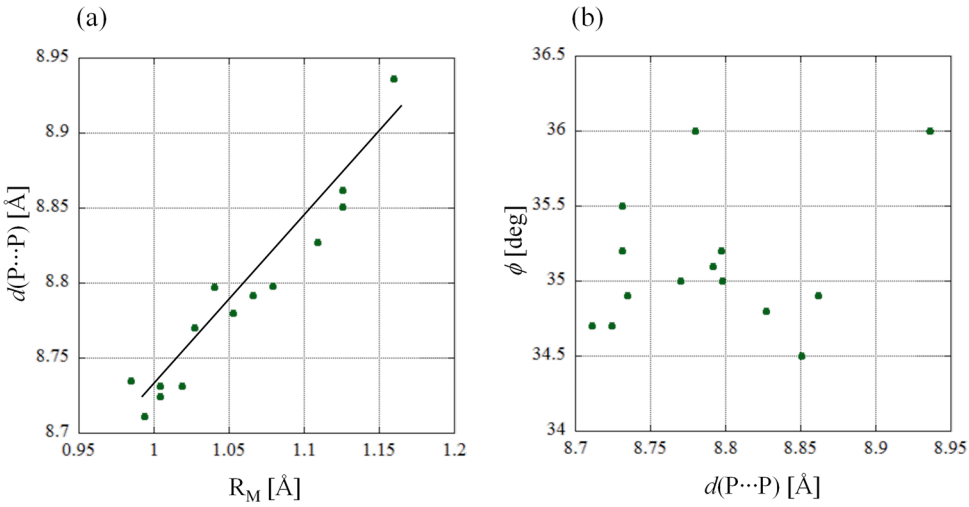

Figure 6. Plots of the (a) ionic radius of M (R_M) versus P···P distance (d(P···P)) and (b) d(P···P) versus twist angle (ϕ) for the $[M(\alpha\text{-}PW_{11}O_{39})_2]^{n-}$ polyanion in the Na^+/K^+-mixed salt containing Pro family given in Table 2. The solid line in each plot is drawn to guide the correlation.

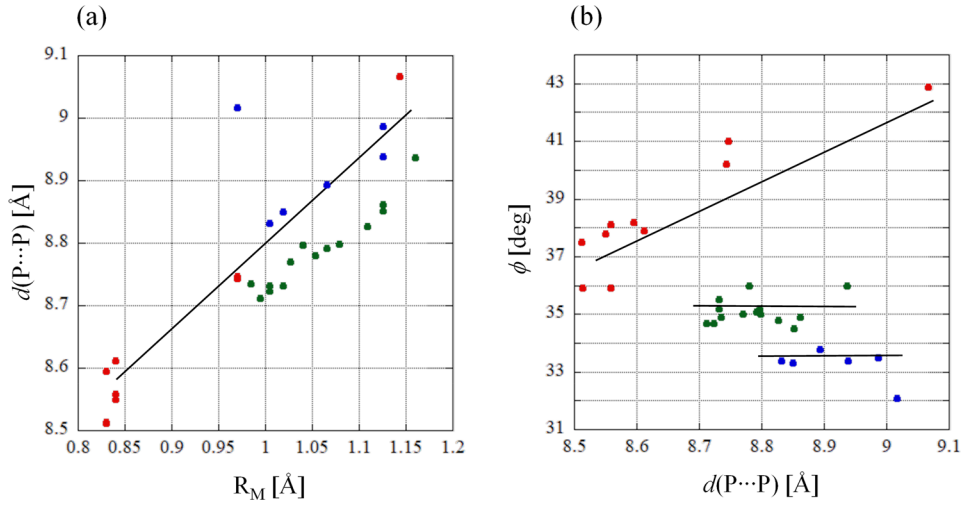

Figure 7. Plots of the (a) ionic radius of M (R_M) versus P···P distance (d(P···P)) and (b) d(P···P) versus twist angle (ϕ) for all the $[M(\alpha\text{-}PW_{11}O_{39})_2]^{n-}$ polyanions given in Table 2. The solid line in each plot is drawn to guide the correlation. The red, green, and blue spheres are the plots corresponding to pure alkylammonium salt family, TMA^+/Na^+-mixed salt family, and Na^+/K^+-mixed salt containing Pro family, respectively.

$[Me_4N]_6Na_5[Er(\alpha\text{-}PW_{11}O_{39})_2]\cdot 19H_2O$ (**TN-Er(III)**), $[Me_4N]_6Na_5[Y(\alpha\text{-}PW_{11}O_{39})_2]\cdot 22.5H_2O$ (**TN-Y(III)**), and $[Me_4N]_6Na_2(NH_4)_2[Ce(\alpha\text{-}PW_{11}O_{39})_2]\cdot 14H_2O$ (**TN-Ce(IV)**)[33] (see also Table 2). As shown in Figure 5a, with the exception of **TN-Ce(IV)**, d(P···P) tends to increase with an increase in R_M[36] because of stretching of the M−O bonds. In addition, Figure 5b displays the correlation between d(P···P) and ϕ, indicating that ϕ is considerably smaller than in the case of the polyanions of the pure alkylammonium salts, although it remains relatively constant upon variation in d(P···P), again with the exception of **TN-Ce(IV)**. It should be noted that the ϕ value of **TN-Ce(IV)** was found to be significantly smaller than those of the other four compounds (ϕ = 32.1°). In contrast to the results obtained for the pure alkylammonium salt family, $d(O_A\cdots O_{A'})$ was large and almost invariable (3.21(2)−3.37(2) Å) for all compounds except for **TN-Ce(IV)** (Table 2). As shown in Figure 2, the two $[\alpha\text{-}PW_{11}O_{39}]^{7-}$ units that form the polyanions in **TN-Pr(III)**, **TN-Eu(III)**, **TN-Er(III)**, and **TN-Y(III)** are locked by interactions between Na^+ cations and the O_A and $O_{A'}$ atoms to produce a $NaO_AO_{A'}$ triangle. Due to the fact that Na^+ cations tend to form rigid NaO_6 octahedra, the constant $d(O_A\cdots O_{A'})$ value can be attributed to this Na^+ cation, which fixes $d(O_A\cdots O_{A'})$ at relatively large values, resulting in a low and constant twist angle (ϕ) (Figure 5b). Notably, the corresponding parameter of **TN-Ce(IV)** deviates exceptionally from this tendency. This can be attributed to the fact that **TN-Ce(IV)** does not possess any locking Na^+ cation to link the O_A and $O_{A'}$ atoms; instead, the polyanions are connected by Na^+ to form a *zigzag* chain running along the longitudinal direction of the polyanion.[33] Such directional connections by Na^+ effectively increase the distance between the two $[\alpha\text{-}PW_{11}O_{39}]^{7-}$ units, as can be seen by the remarkably long d(P···P) (*i.e.*, 9.02(1) Å) for **TN-Ce(IV)** (Table 2). In this case, the $O_A\cdots O_{A'}$ repulsion was reduced ($d(O_A\cdots O_{A'})$ = 3.48(1) Å), and φ was affected by repulsion among all three O···O contacts (*i.e.*, $O_A\cdots O_{A'}$, $O_A\cdots O_{B'}$, and $O_{A'}\cdots O_B$). In fact, the three O···O contacts in **TN-Ce(IV)** were found to be approximately equidistant (*i.e.*, 3.48(1)−3.54(1) Å), thereby minimizing the overall O···O repulsion (Table 2).

https://doi.org/10.1021/acsomega.3c00711
ACS Omega 2023, 8, 9673−9683

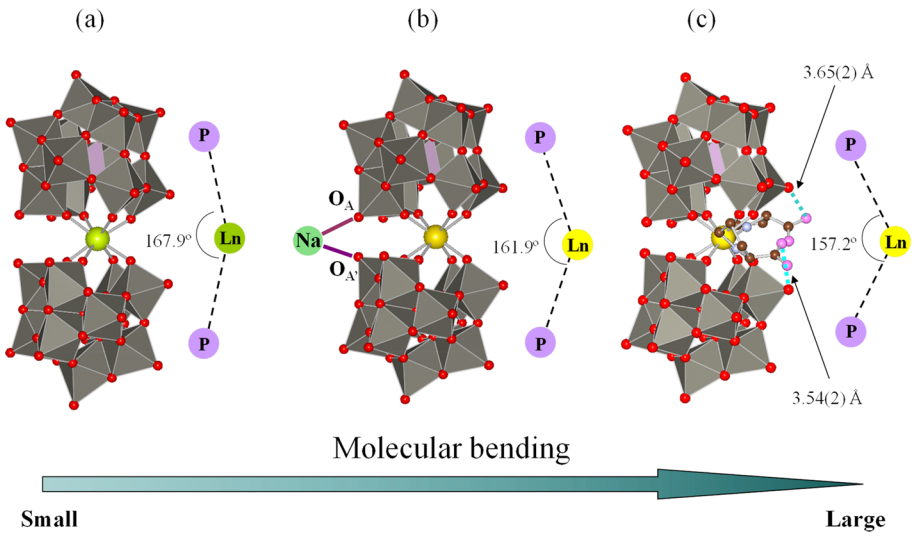

Figure 8. Difference in molecular bending (∠P−M−P′ = φ) in the polyanions. Polyanions in (a) the pure alkylammonium salt family, (b) the TMA^+/Na^+-mixed salt family, and (c) the Na^+/K^+-mixed salt containing Pro family. The polyanions are represented by a combined polyhedral and ball-and-stick representation . Color scheme: WO_6, gray octahedra; PO_4, purple tetrahedra; O atoms, red spheres; O atoms in Pro molecule, pink spheres; M atoms, light green and yellow spheres; Na atoms, green spheres; N atoms, light blue spheres; C atoms, brown spheres. The Na−O bonds and O···O steric repulsion between $[\alpha\text{-}PW_{11}O_{39}]^{7-}$ and carboxyl group in Pro are denoted by bold purple lines and dashed blue lines, respectively.

Structural Evaluation of the Pro-Containing Na^+/K^+-Mixed Salt Family. Figure 6 shows the relationship among the selected geometric parameters of $K_{1.3}Na_{3.2}H_{6.5}[Ln(\alpha\text{-}PW_{11}O_{39})_2]\cdot 8.3(L\text{-}/D\text{-}C_5H_9NO_2;\ Pro)\cdot xH_2O$ (Ln = Pr, **NK-Pr(III)-L** and **-D**; Ln = Nd, **NK-Nd(III)-L**; Ln = Sm, **NK-Sm(III)-L**; Ln = Gd, **NK-Gd(III)-L**; Ln = Tb, **NK-Tb(III)-L**; Ln = Dy, **NK-Dy(III)-L**; Ln = Er, **NK-Er(III)-L** and **-D**; Ln = Tm, **NK-Tm(III)-L**; Ln = Yb, **NK-Yb(III)-L**; Ln = Y, **NK-Y(III)-L**; $K_{1.2}Na_2H_{7.8}[Ln(\alpha\text{-}PW_{11}O_{39})_2]\cdot 8.5(L\text{-}C_5H_9NO_2;\ Pro)\cdot xH_2O$ (Ln = La, **NK-La(III)-L**; Ln = Eu, **NK- Eu(III)-L**)[34,35] (see also Table 2). As shown in Figure 6a, d(P···P) tends to increase with an increase in R_M due to stretching of the M−O bonds, as observed also for the pure alkylammonium and TMA^+/Na^+-mixed salt families (Figures 4a and 5a, respectively). In addition, Figure 6b shows the correlation between d(P···P) and ϕ, wherein no clear trend or correlation can be observed. This behavior can be explained by considering the local structures of the polyanions. As previously reported,[33,34] two Pro molecules exist around the LnO_8 center to form a complex (e.g., L-/D-$[Ln(\alpha\text{-}PW_{11}O_{39})_2]^{11-}$-(L-/D-Pro)$_2$) through hydrogen bonding and stereoselective interactions between the Pro molecules and the surfaces of the polyanion "grooves". More specifically, four hydrogen bonds between the N atoms of Pro and the O atoms of LnO_8 stabilize the SA conformation of Ln^{3+} and contribute to chiral isolation.[34,35] These Pro molecules therefore play a greater role in determining the value of ϕ than the Ln^{3+} species (Table 2 and Figure 6). It should be noted that the contribution of the $O_A\cdots O_{A'}$ repulsion in this series is smaller due to the fact that the Pro molecules fix ϕ at a low value (34.5(1)−36.0(2)°), resulting in a relatively large $d(O_A\cdots O_{A'})$ (*i.e.*, 2.87(4)−3.06(2) Å) with a weak R_M dependence (Table 2).

Comparison of the Molecular Conformations of $[M(\alpha\text{-}PW_{11}O_{39})_2]^{n-}$ in a Variety of Cationic Environments and in the Presence of Coexisting Compounds. As shown in Figure 7a, d(P···P) tends to increase with increasing R_M for all series of $[M(\alpha\text{-}PW_{11}O_{39})_2]^{n-}$ polyanions, irrespective of the cationic species and coexisting compounds that are present. This tendency indicates that d(P···P) is effectively ruled by R_M owing to lanthanide contraction. On the other hand, the plots of d(P···P) vs ϕ show two tendencies (Figure 7b). More specifically, for the pure alkylammonium salts (red plots), φ decreased with a reduction in d(P···P) because of the $O_A\cdots O_{A'}$ steric repulsion produced by the approaching $[\alpha\text{-}PW_{11}O_{39}]^{7-}$ units. In contrast, for the TMA^+/Na^+-mixed salt (blue plots) and Na^+/K^+-mixed salt families (green plots), ϕ was relatively low and constant, and it tended to exhibit no correlation with d(P···P). This observation is attributable to the fixation of ϕ at small values by the attachment of Na^+ and Pro molecules to the $[\alpha\text{-}PW_{11}O_{39}]^{7-}$ units via Na−O bonding and hydrogen bonding, respectively (Figure 8b,c). Such external anisotropic forces in the TMA^+/Na^+-mixed salts and the Pro-containing Na^+/K^+-mixed salts are stronger than the isotropic hydrogen bonding present in the pure alkylammonium salts, and these forces precede the $O_A\cdots O_{A'}$ steric repulsion. In fact, the generation of Na^+ linkages or the insertion of Pro into the polyanion groove influences not only ϕ but also the degree of molecular bending. As shown in Figure 8, the ∠P−M−P angle (φ) indicates that the intramolecular bending of the $[M(\alpha\text{-}PW_{11}O_{39})_2]^{n-}$ polyanion decreased to 167.9, 161.7, and 157.2° in the order of the pure alkylammonium, TMA^+/Na^+-mixed salt, and Pro-containing Na^+/K^+-mixed salt families, respectively. The smaller values of φ (blue plots) obtained for the TMA^+/Na^+-mixed salts (see Figure 9a) can be interpreted by considering the presence of strong Na−O bonds, whereas the smallest values of φ (green plots) for the Pro-containing Na^+/K^+-mixed salt family (see Figure 9a) can be explained by considering the insertion of the two Pro molecules into the groove of the polyanion. In the latter case, other O···O interactions (with distances of 3.65(2) and 3.54(2) Å, represented by the light blue broken lines in Figure 8c) between the carboxylate O atoms and the polyanion terminal also contribute to the distortion. The corresponding plots of φ vs ϕ are shown in Figure 9a. For the TMA^+/Na^+-mixed salt (blue plots) and Pro-containing Na^+/K^+-mixed salt families

https://doi.org/10.1021/acsomega.3c00711
ACS Omega 2023, 8, 9673−9683

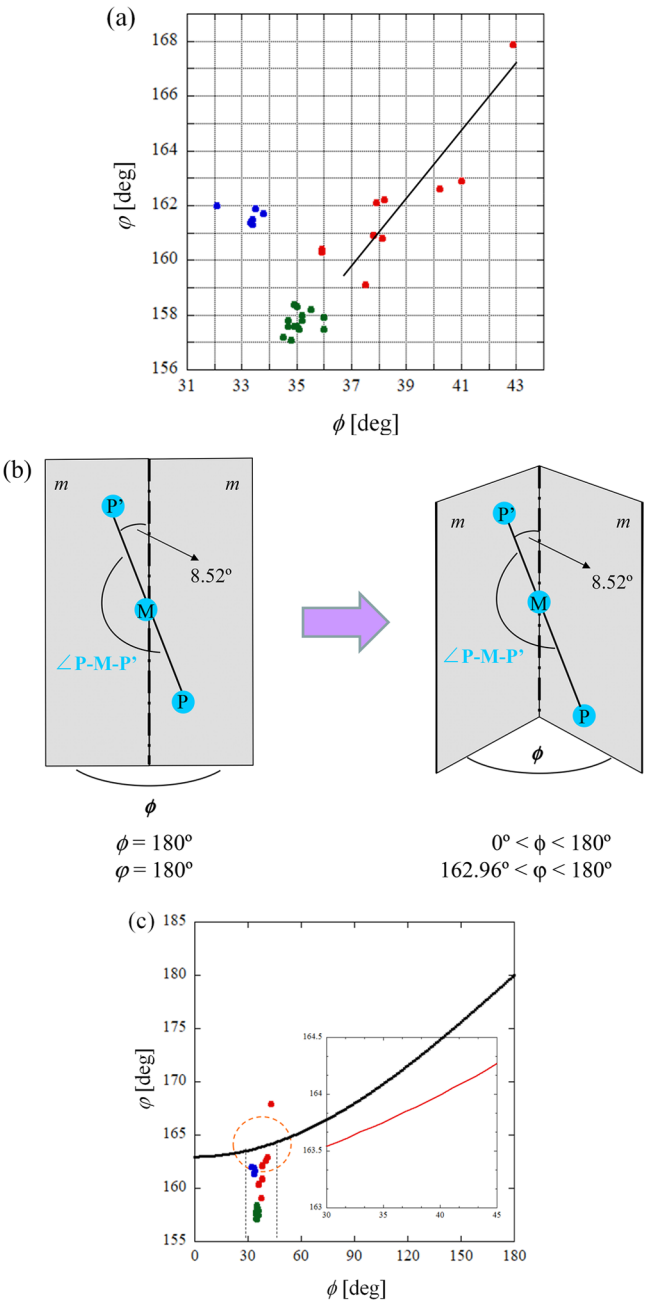

Figure 9. (a) Plots of the molecular bending (∠P−M−P′ = φ) versus twist angle (ϕ) for all of the $[M(\alpha\text{-}PW_{11}O_{39})_2]^{n-}$ polyanions given in Table 2. The red, blue, and green spheres correspond to the pure alkylammonium salt family, TMA^+/Na^+-mixed salt family, and Na^+/K^+-mixed salt containing Pro family, respectively. (b) Definition of ϕ and φ based on the geometrical modeling considering the genuine rotation effect of $[\alpha\text{-}PW_{11}O_{39}]^{7-}$. (c) Plots of φ versus ϕ based on the geometrical modeling mentioned above. The inset gives an expansion of the orange dotted circled region. The red, blue, and green spheres are the plots corresponding to the pure alkylammonium salt family, TMA^+/Na^+-mixed salt family, and Na^+/K^+-mixed salt containing Pro family, respectively.

(green plots), both φ and ϕ remained relatively constant due to immobilization of the $[\alpha\text{-}PW_{11}O_{39}]^{7-}$ units by Na−O bonding and Pro insertion, respectively. In contrast, φ tended to decrease with a decrease in φ for the pure alkylammonium family (red plots). This observation indicates that the $[\alpha\text{-}PW_{11}O_{39}]^{7-}$ units are not effectively fixed by the weak hydrogen bonding involving the alkylammonium cations and crystallization water molecules.

Subsequently, the geometrical relationship between φ and ϕ was estimated using a simple $[\alpha\text{-}PW_{11}O_{39}]^{7-}$ rotation model (Figure 9b). The $[Ce^{III}(\alpha\text{-}PW_{11}O_{39})_2]^{11-}$ polyanion, which possesses a cubic-coordinated CeO_8 center,[19] was used as the starting model and has an ideal geometry of φ = 180° and ϕ = 180°. The rotation axis of the $[\alpha\text{-}PW_{11}O_{39}]^{7-}$ unit was defined such that it passed through the Ce atom and was normal to the O_4 square plane coordinating to Ce in the CeO_8 center. In this case, the angle between the Ce···P vector and the rotation axis was measured to be 8.52°. When φ was reduced from 180° to 0°, φ was also reduced from 180 to 162.96° according to the equation $\varphi = \cos^{-1}[-(a^2 \cos \varphi + b^2)]$ (a^2 and b^2 are constants), which is represented by the black curve in Figure 9c. This reveals that in the range of ∼30° < ϕ < 45° for the SA coordination (Figure 9c, inset), φ should exhibit only a small variation: *i.e.*, from 163.5 to 164.3°. Thus, ϕ makes little contribution to the determination of φ when only the rotation effect of the $[\alpha\text{-}PW_{11}O_{39}]^{7-}$ units is considered. However, the plots obtained for the pure alkylammonium salt family demonstrated a remarkably wider range of 159.1° < φ < 167.9° (red plots in Figure 9c), which was attributed to both intramolecular and external molecular factors acting on the flexible conformation of the polyanions in this family. Overall, these results indicate that the geometrical parameters of φ and ϕ are greatly affected by the value of R_M, the cationic environment, and the interacting molecules (Pro in the case of the current study) but are almost independent of the rotation effect of $[\alpha\text{-}PW_{11}O_{39}]^{7-}$. These results demonstrate the rigidity of the $[\alpha\text{-}PW_{11}O_{39}]^{7-}$ unit and the flexibility of LnO_8 coordination. Due to the fact that such molecular bending has a small effect on the $O_A \cdots O_{A'}$ contacts, its evaluation was not possible irrespective of the other geometric parameters.

■ CONCLUSIONS

A clear correlation between the ionic radius (R_M) of the central metal atom (M) and the twist angle (ϕ) of the two monolacunary $[\alpha\text{-}PW_{11}O_{39}]^{7-}$ units was demonstrated for a series of $[M(\alpha\text{-}PW_{11}O_{39})_2]^{n-}$ polyanions in the presence of a variety of cationic and coexisting molecular environments. This observation was explained in terms of not only the steric repulsion between the O atoms in the two monolacunary $[\alpha\text{-}PW_{11}O_{39}]^{7-}$ units but also the molecular environment surrounding the polyanion, including the cation arrangement and the presence of coexisting compounds. The obtained results demonstrated that some interactions between the polyanion and its countercations and coexisting compounds ultimately determine the coordination environment of Ln and the resulting isolated form (racemate or enantiomer). To further investigate the stable molecular geometries of Ln polyoxometalates (Ln-POMs) in terms of such intra- and intermolecular interactions, theoretical approaches based on quantum mechanics are required. However, in modern chemistry, geometric discussions using molecular models based on the results obtained from single-crystal X-ray diffraction analysis are the limit. Therefore, complete *ab initio* calculations of the molecular scales of $[M(\alpha\text{-}PW_{11}O_{39})_2]^{n-}$ and larger Ln-POM analogues, such as $[M(\alpha_2\text{-}P_2W_{17}O_{61})_2]^{n-}$ and their cationic surroundings will remain a challenging task in this area for a long time.

https://doi.org/10.1021/acsomega.3c00711
ACS Omega 2023, 8, 9673−9683

■ ASSOCIATED CONTENT

Supporting Information

The Supporting Information is available free of charge at https://pubs.acs.org/doi/10.1021/acsomega.3c00711.

Crystallographic data for **TN-Pr(III)** (CCDC-812378) (CIF)

Crystallographic data for **TN-Eu(III)** (CCDC-1945568) (CIF)

Crystallographic data for **TN-Er(III)** (CCDC-812380) (CIF)

Crystallographic data for **TN-Y(III)** (CCDC-1936822) (CIF)

Crystallographic data for **aa-Ce(IV)-b** (CCDC-2008002) (CIF)

■ AUTHOR INFORMATION

Corresponding Author

Jun Iijima − *Department of Engineering, Tokyo University of Agriculture and Technology, Koganei city, Tokyo 184-8588, Japan*; orcid.org/0000-0002-3469-857X; Email: fr7886@go.tuat.ac.jp; Fax: +81 80 5503 2761

Authors

Haruo Naruke − *University Research Administrator (URA), Tokyo Institute of Technology, Meguro-ku, Tokyo 152-8550, Japan*

Ryuta X. Suzuki − *Department of Engineering, Tokyo University of Agriculture and Technology, Koganei city, Tokyo 184-8588, Japan*

Complete contact information is available at: https://pubs.acs.org/10.1021/acsomega.3c00711

Author Contributions

The manuscript was written through contributions of all authors. All authors have given approval to the final version of the manuscript. H.N. and R.X.S. contributed equally.

Notes

The authors declare no competing financial interest.

■ ACKNOWLEDGMENTS

This work was partly supported by a Sasakawa Scientific Research Grant (28-316) from the Japan Science Society. We are grateful to Professor Yuichiro Nagatsu of the Tokyo University of Agriculture and Technology for his experimental support. We also thank Editage (www.editage.jp) for English language editing.

■ REFERENCES

(1) Hill, C. L. Introduction: Polyoxometalates-Multicomponent Molecular Vehicles to Probe Fundamental Issues and Practical Problems. *Chem. Rev.* **1998**, *98* (1), 1−2. (topical issue on polyoxometalates)

(2) Pope, M. T. *Heteropoly and Isopoly Oxometalates*; Springer: 1983.

(3) Bassil, B. S.; Dickman, M. H.; Römer, I.; von der Kammer, B.; Kortz, U. The Tungstogermanate $[Ce_{20}Ge_{10}W_{100}O_{376}(OH)_4(H_2O)_{30}]^{56-}$: A Polyoxometalate Containing 20 Cerium(III) Atoms. *Angew. Chem., Int. Ed. Engl.* **2007**, *46* (32), 6192−6195.

(4) Naruke, H.; Yamase, T. $Na_8H_{18}[\{Er_3O(OH)_3(H_2O)_3\}_2Al_2(Nb_6O_{19})_5]\cdot 40.5H_2O$. *Acta Crystallogr. C Cryst. Struct. Commun.* **1996**, *52* (11), 2655−2660.

(5) Peacock, R. D.; Weakley, T. J. R. Heteropolytungstate Complexes of the Lanthanide Elements. Part I. Preparation and Reactions. *J. Chem. Soc. A* **1971**, *0*, 1836−1839.

(6) Wassermann, K.; Dickman, M. H.; Pope, M. T. Self-Assembly of Supramolecular Polyoxometalates: The Compact, Water-Soluble Heteropolytungstate Anion $[As_{12}Ce_{16}(H_2O)_{36}W_{148}O_{524}]^{76-}$. *Angew. Chem., Int. Ed. Engl.* **1997**, *36* (1314), 1445−1448.

(7) Fukaya, K.; Yamase, T. Alkali-Metal-Controlled Self-Assembly of Crown-Shaped Ring Complexes Of Lanthanide/ $[\alpha\text{-}AsW_9O_{33}]^{9-}$: $[K\subset\{Eu(H_2O)_2(\alpha\text{-}AsW_9O_{33})\}_6]^{35-}$ and $[Cs\subset Eu(H_2O)_2(\alpha\text{-}AsW_9O_{33})_4\}]^{23-}$. *Angew. Chem., Int. Ed.* **2003**, *42*, 654−658.

(8) Rosu, C.; Weakley, T. J. R. Redetemination of Sodium [Bis(Pentatungstato)Cerate(IV)]. *Acta Crystallogr. C Cryst. Struct. Commun.* **1998**, *54* (9), IUC9800047.

(9) Ozeki, T.; Yamase, T. Effect of Lanthanide Contraction on the Structure of the Decatungstolanthanoate Anions in $K_3Na_4H_2[LnW_{10}O_{36}]\cdot nH_2O$ (Ln = Pr, Nd, Sm, Gd, Tb, Dy) Crystals. *Acta Crystallogr. B Struct. Sci.* **1994**, *50* (2), 128−134.

(10) Sugeta, M.; Yamase, T. Crystal Structure and Luminescence Site of $Na_9[EuW_{10}O_{36}]\cdot 32H_2O$. *Bull. Chem. Soc. Jpn.* **1993**, *66* (2), 444−449.

(11) AlDamen, M. A.; Cardona-Serra, S.; Clemente-Juan, J. M.; Coronado, E.; Gaita-Ariño, A.; Martí-Gastaldo, C.; Luis, F.; Montero, O. Mononuclear Lanthanide Single Molecule Magnets Based on the Polyoxometalates $[Ln(W_5O_{18})_2]^{9-}$ and $[Ln(\beta_2\text{−}SiW_{11}O_{39})_2]^{13-}$ (Ln = Tb, Dy, Ho, Er, Tm, and Yb). *Inorg. Chem.* **2009**, *48* (8), 3467−3479.

(12) Zhang, C.; Howell, R. C.; Scotland, K. B.; Perez, F. G.; Todaro, L.; Francesconi, L. C. Aqueous Speciation Studies of Europium(III) Phosphotungstate. *Inorg. Chem.* **2004**, *43* (24), 7691−7701.

(13) Copping, R.; Gaunt, A. J.; May, I.; Sarsfield, M. J.; Collison, D.; Helliwell, M.; Denniss, I. S.; Apperley, D. C. Trivalent Lanthanide Lacunary Phosphomolybdate Complexes: A Structural and Spectroscopic Study Across the Series $[Ln(PMo_{11}O_{39})_2]^{11-}$. *Dalton Trans.* **2005**, No. 7, 1256−1262.

(14) Mialane, P.; Dolbecq, A.; Riviere, E.; Morrot, J.; Secheresse, F. Functionalization of Polyoxometalates by a Negatively Charged Bridging Ligand: The Dimeric $[(SiW_{11}O_{39}Ln)_2(\mu\text{-}CH_3COO)_2]^{12-}$ (Ln = Gd^{III}, Yb^{III}) Complexes. *Eur. J. Inorg. Chem.* **2004**, *2004*, 33−36.

(15) Jiang, N.; Xu, L.; Li, F.; Gao, G.; Fan, L. A Novel Sandwich Polyoxotungstogermanate: Synthesis, Crystal Structure and Magnetic Property of $[Pr(GeW_{11}O_{39})_2]^{13-}$. *Inorg. Chem. Commun.* **2008**, *11* (1), 24−27.

(16) Fedotov, M. A.; Pertsikov, B. Z.; Danovich, D. K. O, ^{31}P and ^{183}W NMR Spectra of Paramagnetic Complexes with the Heteropolytungstate Anion $[Ln(PW_{11}O_{39})_2]^{11-}$ and Their Constitution in Aqueous Solution, Ln-Rare Earth Element. *Polyhedron* **1990**, *9* (10), 1249−1256.

(17) Copping, R.; Jonasson, L.; Gaunt, A. J.; Drennan, D.; Collison, D.; Helliwell, M.; Pirttijarvi, R. J.; Jones, C. J.; Huguet, A.; Apperley, D. C.; Kaltsoyannis, N.; May, I. Tetravalent Metal Complexation by Keggin and Lacunary Phosphomolybdate Anions. *Inorg. Chem.* **2008**, *47* (13), 5787−5798.

(18) Bartis, J.; Sukal, S.; Dankova, M.; Kraft, E.; Kronzon, R.; Blumenstein, M.; Francesconi, L. C. Lanthanide Complexes of Polyoxometalates: Characterization by tungstten-183 and Phosphorus-31 Nuclear Magnetic Resonance Spectroscopy. *J. Chem. Soc., Dalton Trans.* **1997**, *0* (11), 1937−1944.

(19) Iijima, J.; Naruke, H. Structural Characterization of Keggin Sandwich-Type $[Ln^{III}(\alpha\text{-}PW_{11}O_{39})_2]^{11-}$ (Ln = La and Ce) Anion Containing a Pseudo-Cubic $Ln^{III}O_8$ Center. *Inorg. Chim. Acta* **2011**, *379* (1), 95−99.

(20) Ginsburg, A. P. *Inorg. Synth.* **1990**, *57*, 96.

(21) Higashi, T. *SHAPE-Program to Obtain Crystal Shape Using CCD Camera*; Rigaku Corporation: 1999.

(22) Higashi, T. *NUMABS-Numerical Absorption Correction*; Rigaku Corporation: 1999.

(23) SHELXS Version 2013/1: Sheldrick, G. M. A Short History of SHELX. *Acta Crystallogr. A* **2008**, *64* (1), 112−122.

(24) SHELXL, version 2014: Sheldrick, G. M. A short History of SHELX. *Acta Crystallogr. A: Found. Crystallogr.* **2008**, *64* (64), 112−122.
(25) *CrystalStructure Analysis Package*; Rigaku Corporation: 2000−2016.
(26) The H atoms are not contained in the structural analysis due to their very low electron density. The polyanion in this study consists of 22 tungsten atoms; thus, light atoms such as H atoms are hardly observed. Thus, the H atoms in polyoxomelatate compounds are generally excluded in the refinement process.
(27) Flack, H. D. On Enantiomorph-Polarity Estimation. *Acta Crystallogr. A Found. Crystallogr.* **1983**, *39* (6), 876−881.
(28) http://www.chem.gla.ac.uk/~louis/software/platon/http://www.chem.gla.ac.uk/~louis/software/platon/.
(29) Iijima, J.; Ishikawa, E.; Nakamura, Y.; Naruke, H. Synthesis and Structural Investigation of Sandwich Polyoxotungstates Containing Cerium (III/IV) and Mono-lacunary Keggin Tungstophosphate Units. *Inorg. Chim. Acta* **2010**, *363* (7), 1500−1506.
(30) Hou, Y.; Fang, X.; Hill, C. L. Breaking Symmetry: Spontaneous Resolution of a Polyoxometalate. *Chemistry* **2007**, *13* (34), 9442−9447.
(31) Cai, L.; Li, Y.; Yu, C.; Ji, H.; Liu, Y.; Liu, S. Spontaneous Resolution of a Chiral Polyoxometalate: Synthesis, Crystal Structures and Properties. *Inorg. Chim. Acta* **2009**, *362* (8), 2895−2899.
(32) Kato, C. N.; Shinohara, A.; Hayashi, K.; Nomiya, K. Syntheses and X-ray Clysta1 Structures of Zirconium(IV) and Hafnium (IV). *Inorg. Chem.* **2006**, *45* (20), 8108−8119.
(33) Fan, L.; Xu, L.; Gao, G.; Li, F.; Li, Z.; Qiu, Y. A Novel Polyoxometalate Chain Constructed from Sandwich Lanthanide-Containing Polyanion $[Ce(PW_{11}O_{39})_2]^{10-}$ and Sodium Ion Linker. *Inorg. Chem. Commun.* **2006**, *9* (12), 1308−1311.
(34) Naruke, H.; Iijima, J.; Sanji, T. Enantioselective Resolutions and Circular Dichroism Studies of Lanthanide-Containing Keggin-Type $[Ln(PW_{11}O_{39})_2]^{11-}$ Polyoxometalates. *Inorg. Chem.* **2011**, *50* (16), 7535−7539.
(35) Iijima, J.; Naruke, H.; Sanji, T. On Chirality Induction in the Crystalline Solid-Containing Sandwich-Type $[Ln(\alpha\text{-}PW_{11}O_{39})_2]^{11-}$ Polyoxotungstate and Proline. *R.S.C. Adv.* **2016**, *6* (94), 91494−91507.
(36) Shannon, R. D. Revised Effective Ionic Radii and Systematic Studies of Interatomic Distances in Halides and Chalcogenides. *Acta Cryst. A* **1976**, *32* (5), 751−767.
(37) Fang, X.; Anderson, T. M.; Neiwert, W. A.; Hill, C. L. Yttrium Polyoxometalates. Synthesis and Characterization of a Carbonate-Encapsulated Sandwich-Type Complex. *Inorg. Chem.* **2003**, *42* (26), 8600−8602.
(38) Brown, I. D. In *Structure and Bonding in Crystals*; O'Keeffe, M., Navrotsky, A., Eds.; Academic Press: 1980; pp 1−29.
(39) Fan, L. H.; Xu, L.; Zhang, C. H.; Li, F. Y.; Li, Z. K.; Liu, X. Z. A Novel Polyoxometalate Chain Constructed from Sandwich Lanthanide-Containing Polyanions $[Pr(PW_{11}O_{39})_2]^{11-}$ and Sodium Linkers. *Struct. Chem.* **2007**, *18* (6), 917−921.

https://doi.org/10.1021/acsomega.3c00711
ACS Omega 2023, 8, 9673−9683